

THERMOPHYSICAL PROPERTIES OF Gd DOPED CERIA NANOPARTICLES

A. S. SALEEMI^{a,b}, A. ABDULLAH^{a,c}, M. ANIS-UR-REHMAN^{a*}

^a*Applied Thermal Physics Laboratory, Department of Physics, COMSATS Institute of Information Technology, Islamabad 44000, Pakistan*

^b*Key Laboratory of Advanced Materials (MOE), School of Materials Science and Engineering, Tsinghua University, Beijing, People's Republic of China and Beijing National Center for Electron Microscopy, Beijing 100084, People's Republic of China*

^c*School of Science, University of Management and Technology, Sialkot Campus, Sialkot 51310, Pakistan*

Composite mediated hydrothermal (CMH) method, a facile technique to prepare functional materials, was utilized to synthesize the nanocrystalline gadolinium doped ceria. The structural properties and surface morphology for the composition $Ce_{1-x}Gd_xO_\delta$ ($x = 0.10, 0.15, 0.20, 0.25$) were studied by x-ray diffraction (XRD) and scanning electron microscopy (SEM). The Raman spectroscopy was performed to verify the Gd doping in ceria. The crystallite size was estimated by Scherrer's and Stokes and Wilson's formulae and the minimum size obtained, corresponding to most intense peak was 30 nm for $Ce_{0.85}Gd_{0.15}O_\delta$ calculated with Scherrer formula. The lattice constant measurements were done using x-ray diffraction data. AC and DC conduction studies were done on pellets. DC conductivity was measured in temperature range 300-700 °C. Activation energies were calculated from Arrhenius plots and were in range 0.87-1.19 eV. AC conductivity was measured as a function of frequency (1 kHz to 3 MHz) at different temperatures (300, 400, 500, 600, and 700 °C). The conductivity value was achieved as high as $9.30 \times 10^{-4} S \cdot cm^{-1}$ at 600 °C for $Ce_{0.75}Gd_{0.25}O_\delta$. The thermal conductivity and thermal diffusivity values were also determined. The synthesis of electrolyte materials for intermediate temperature solid oxide fuel cells (ITSOFCs) was found to be better with composite mediated hydrothermal method.

(Received October 9, 2016; Accepted January 11, 2017)

Keywords: Crystallization; Powder diffraction; Raman spectroscopy; Dielectric properties; Microstructure; Transport properties

1. Introduction

The fuel cells promise the silent, proficient and uncontaminated power through the conversion of chemical energy into electrical. The solid oxide fuel cells (SOFCs), having variety of working temperature ranges, are of considerable interest among others [1-5]. Ceria and doped ceria compounds are being utilized as electrolyte material in the intermediate temperature solid oxide fuel cells (ITSOFCs) among others to improve the conductivity besides their other applications [5]. The conductivity of the electrolyte can be enhanced by tuning the factors like synthesis technique, particle size, composition and dopants [6]. In recent years, researchers have been working on different compositions, dopants and synthesis methods experimentally [6-18] and predicting the behaviors through models [19-22]. Herein, the synthesis and conduction properties of gadolinium doped ceria are presented. A facile method, composite mediated hydrothermal (CMH) method, was adopted to synthesize the material in nanocrystalline phase. The doping concentration of Gd in CeO_2 was varied and DC conductivity and activation energy were observed in temperature range 300-700 °C. The frequency dependent response was also observed in

* Corresponding author: marehman@comsats.edu.pk

frequency range 1 kHz to 3 MHz at temperatures 300, 400, 500, 600 and 700 °C. The increase in conductivity values is considered to be due to change in the microstructures and availability of oxygen vacancies with dopant contents.

2. Experimental

2.1 Materials and Method

The precursors for the ceria-gadolinia system were cerium nitrate and gadolinium nitrate ($\text{Ce}(\text{NO}_3)_3 \cdot 6\text{H}_2\text{O}$ and $\text{Gd}(\text{NO}_3)_3 \cdot 6\text{H}_2\text{O}$). The potassium hydroxide and sodium hydroxide (KOH & NaOH) were used as precipitating agents. All chemicals were of Sigma-Aldrich made, of analytical grade and were used as purchased. The CMH method was utilized to get $\text{Ce}_{1-x}\text{Gd}_x\text{O}_\delta$ ($x = 0.10, 0.15, 0.20, 0.25$). The corresponding samples were nominated as CG10, CG15, CG20 and CG25.

2.2. Synthesis

The CMH method was preferred due to its simplicity of procedure, less impurities (practically zero) in final product and relatively environmental affable. Moreover, very few reports were available for the synthesis of similar materials [6, 23]. The method made used was the eutectic point of NaOH-KOH system. The NaOH and KOH have melting temperatures 323 °C and 406 °C respectively but the NaOH-KOH system at the mole ratio 0.515/0.485 have eutectic point at 170 °C [24-25] i.e. these melt at this temperature for this ratio. By this technique the NaOH-KOH not only served as reactants but also as precipitating agents. For a typical reaction, $\text{Ce}(\text{NO}_3)_3 \cdot 6\text{H}_2\text{O}$, 4.49 g, $\text{Gd}(\text{NO}_3)_3 \cdot 6\text{H}_2\text{O}$, 0.51 g, NaOH, 10.3 g and KOH, 9.7 g were used. All chemicals in powder form were mixed in Teflon chamber, sealed and were heat treated at 180 °C for 45 minutes in a pre-heated resistive heating oven. After the heat treatment, the vessel was allowed to cool to room temperature. The final product was washed with de-ionized water several times and then dried in oven. The calcination was done at 500 °C for 2 h. The pellets, made with this calcined 1g powder of 13mm diameter, were then sintered at 800 °C for 5 h. The pellets were made using hydraulic press. The heating was done at rate of 5 degree per minute and were furnace cooled naturally. These sintered pellets were utilized for further characterizations.

2.3. Growth of Nanocrystalline structures

The nanocrystalline growth could be credited to the chemical potential (maintained through precipitation), pressure and temperature ($T > 100$ °C, $P > 1$ Bar). A simple explanation of the growth could be given using Gibbs-Curie-Wulff model [26]. The model elucidated that the equilibrium state of a crystal is due to the compromise of the free energies of respective faces. The needles-like structures in CG10 (shown in SEM micrographs) could be accredited to relatively high mobility of ions in solution in comparison with other compositions.

2.4. Characterizations

2.4.1. Structural and morphological

The x-ray diffraction patterns were taken on Panalytical X'Pert Pro in 2θ range of 20 to 80 degrees using Cu-K α radiations. The crystallite sizes were estimated using Scherrer formula

$$D = \frac{0.9\lambda}{\beta \cos\theta}, \quad (1)$$

and Stokes and Wilson's formula which incorporate the effects of strains in crystals

$$\beta = \frac{0.9\lambda}{D \cos\theta} + 4\epsilon \tan\theta. \quad (2)$$

The strains were calculated using the relation

$$\epsilon = \frac{\beta \cos \theta}{4}. \quad (3)$$

The lattice constant 'a' of the system was calculated using the relation

$$a = d\sqrt{h^2 + k^2 + l^2}. \quad (4)$$

Raman spectrum was taken with 514 nm laser in the range 400 to 700 cm^{-1} on Dong Woo Optron Raman & PL device. The SEM micrographs were taken on Hitachi SU 1500.

2.4.2 AC and DC measurements

The capacitance and dissipation factor were measured on Wayne Kerr LCR meter 6440B in frequency range 1 kHz to 3 MHz at different temperatures (300 °C, 400 °C, 500 °C, 600 °C and 700 °C) using Cu plates as electrodes, in air. The 4-point measurement technique of LCR meter was employed. The dielectric constant ϵ' was calculated using relation

$$\epsilon' = \frac{Cd}{A\epsilon_0}. \quad (5)$$

The AC conductivity was calculated using the formula

$$\sigma_{ac} = \omega\epsilon_0\epsilon'\tan\delta, \quad (6)$$

where, $\omega = 2\pi f$.

The resistance in the temperature range 300 °C to 700 °C was measured using the same meter with 1 volt applied. The resistivity and then conductivity was calculated by using

$$\rho = \frac{RA}{L}; \quad (7)$$

where, $A = \text{contact area}$, $L = \text{thickness of the pellet}$

2.4.3 Thermal measurements

The thermal conductivity and diffusivity values for these samples were done by employing Advantageous Transient Plane Source (ATPS) method. The thermal diffusivity, thermal conductivity and specific heat are related through

$$\kappa = \frac{\lambda}{\rho C_p} \quad (8)$$

where $\kappa = \text{thermal diffusivity}$, $\lambda = \text{thermal conductivity}$ and the product in denominator is the volumetric heat capacity. The power of heat pulse and change in temperature are related by

$$\overline{\Delta T(\tau)} = \frac{P_0}{r \lambda \pi^{3/2}} D_s(\tau) \quad (9)$$

where $P_0 = \text{power}$, $D_s(\tau) = \text{time dependent temperature increase for disk shaped sensor}$, $\lambda = \text{thermal conductivity}$, r and $D_s(\tau)$ are dimensional parameters of the sensor [27].

3. Results and discussion

3.1 Structural and morphological

The XRD patterns given in Fig. 1 of prepared samples, showed the formation of cubic structure. All peaks were indexed with cubic fluorite structure (space group 225). The crystallite

sizes (corresponding to most intense (111) peak and average) and lattice constant are given in Table 1.

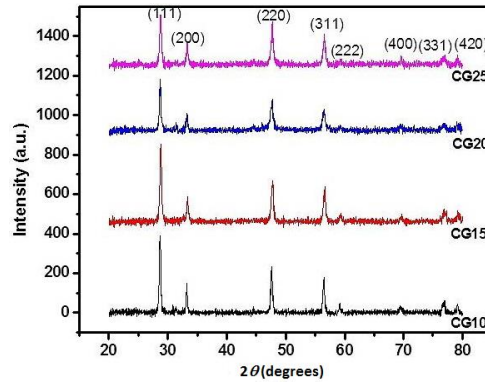


Fig. 1 Indexed X-Ray diffraction patterns of $Ce_{1-x}Gd_xO_\delta$ ($x = 0.10$ (CG10), 0.15 (CG15), 0.20 (CG20), 0.25 (CG25))

Table 1: The crystallite sizes ($D_{s(111)}$) = Crystallite size corresponding most intense peak estimated using Scherrer's formula, $D_{w(111)}$ = Crystallite size, corresponding most intense peak, estimated using Stokes & Wilson's formula, D_s = Average crystallite size estimated by Scherrer's formula, D_w = Average crystallite size estimated by Stokes and Wilson's formula) and lattice constant of $Ce_{1-x}Gd_xO_\delta$ ($x = 0.10$ (CG10), 0.15 (CG15), 0.20 (CG20), 0.25 (CG25))

Sample	$D_{s(111)}$ (nm)	$D_{w(111)}$ (nm)	D_s Average (nm)	D_w Average (nm)	Lattice Constant Å
CG10	66	88	34	76	5.40(2)
CG15	30	40	24	44	5.38(3)
CG20	83	111	32	55	5.40(2)
CG25	83	111	41	76	5.40(3)

The Raman spectra of $Ce_{1-x}Gd_xO_\delta$ are given in Fig. 2. The spectra showed the single intense peak corresponding to the oxygen-cerium F_{2g} mode vibration for cubic fluorite structure at ca. 465 cm^{-1} .

The doping of Gd in Ceria was confirmed from the absence of Raman bands at ca. 480 cm^{-1} which is vibrational mode of cubic Gd_2O_3 . Also, the increase in dopant concentration of the Gd increased the peak bandwidth which was due to the intermixing of bands and increased vacancies [28-29].

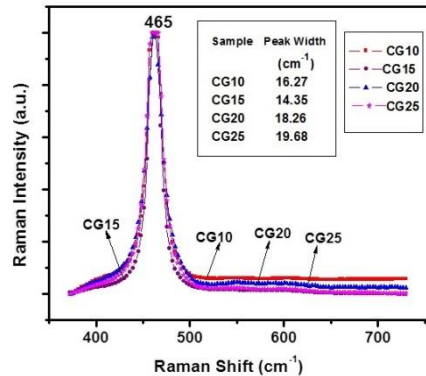


Fig. 2 Raman spectroscopy of $Ce_{1-x}Gd_xO_\delta$ ($x = 0.10$ (CG10), 0.15 (CG15), 0.20 (CG20), 0.25 (CG25))

Table 2: Activation energies and DC conductivities of $Ce_{1-x}Gd_xO_\delta$ ($x=0.10$ (CG10), 0.15 (CG15), 0.20 (CG20), 0.25 (CG25)) at different temperatures

Sample	Activation Energy (eV)	DC Conductivity ($S\text{-cm}^{-1}$)					
		300-700 °C	500 °C	550 °C	600 °C	650 °C	700 °C
CG10	0.89(1)		1.14×10^{-4}	4.02×10^{-4}	6.74×10^{-4}	13.3×10^{-4}	24×10^{-4}
CG15	0.87(1)		4.10×10^{-5}	1.42×10^{-4}	2.10×10^{-4}	2.76×10^{-4}	4.5×10^{-4}
CG20	1.19(2)		2.89×10^{-5}	1.20×10^{-4}	1.57×10^{-4}	4.25×10^{-4}	6.52×10^{-4}
CG25	1.13(2)		1.95×10^{-4}	4.78×10^{-4}	9.30×10^{-4}	25.8×10^{-4}	74×10^{-4}

The SEM micrographs are shown in Fig. 3. The sample CG10 has needles-like structures and the other three samples have coarse particles.

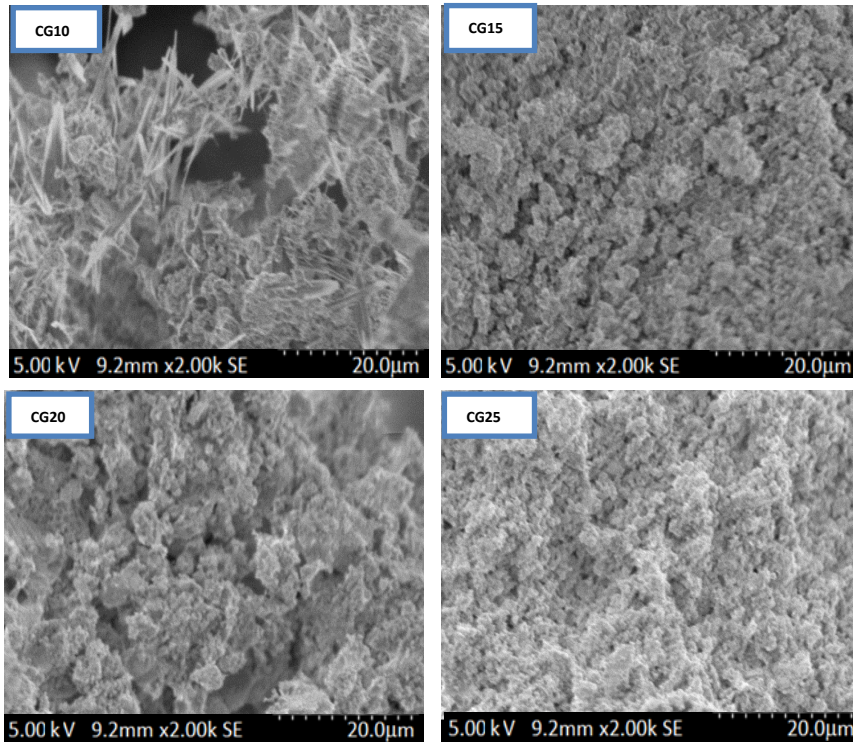


Fig. 3. Scanning electron micrographs of $Ce_{1-x}Gd_xO_\delta$ ($x=0.10$ (CG10), 0.15 (CG15), 0.20 (CG20), 0.25 (CG25))

3.2 DC and AC Conductivity

The DC conductivities of prepared samples are shown in Fig. 4. The activation energies calculated are given in Table 2. The ceria and Gd doped ceria are very high resistive at room temperature. At higher temperature these become conductive and the oxygen ion conductivity is dependent on temperature. The values of conductivities of prepared samples at different temperatures are mentioned in Table 2. The sample CG25 has the highest value of conductivity. The increase in conductivity might be credited to the increase in vacancy sites due to the increase in Gd contents as confirmed from Raman spectroscopy and the microstructure distribution due to the synthesis process. The CG10 has otherwise higher conductivity values which is due to the grain boundary effect. Moreover, coarse grained structure also favored higher conductivities [30-31]. The frequency spectra of $Ce_{1-x}Gd_xO_\delta$ ($x=0.10, 0.15, 0.20, 0.25$) at different temperatures are given in Fig. 5. The behavior could be explained by Jump relaxation model [32-33]. At lower frequencies, the DC conductivity was due to the jumping of ion from one vacant state to other. At higher frequencies dispersion occur due to hopping and relaxation of ions. The increase in temperature, moved the dispersion region toward the high frequency region. The step in dispersion

was the confirmation of grains boundaries and interior conduction. The confirmation of ionic hopping in addition to Arrhenius relation is given by the Jonscher's law [34-37]. The values of AC conductivities at different temperatures and on different applied frequencies are summarized in Table 3. The higher values of AC conductivities confirmed the dominating ionic conduction although the presence of DC conductivity showed the electronic contribution. The conductivity values of these samples synthesized using CMH method are found to be higher than other reports using synthesis methods like thermal decomposition [38], combustion [17], citrate auto ignition [35, 37] and co-precipitation [39].

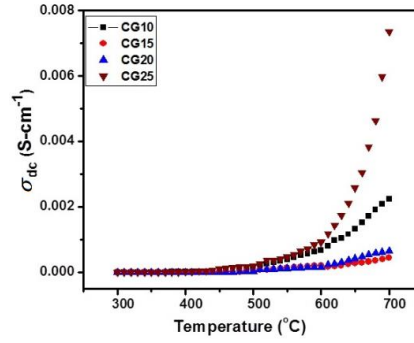


Fig. 4 DC conductivity of $Ce_{1-x}Gd_xO_\delta$ ($x=0.10$ (CG10), 0.15 (CG15), 0.20 (CG20), 0.25 (CG25)) as function of temperature

3.3 Dielectric responses

The dielectric constants as function of frequency are shown in Fig. 6. The 'universal' dielectric response was evident from the plots. The Jonscher's law is applicable to such materials which do not show loss peaks [34-37]. The high values of dielectric constant at lower frequencies were the manifestation of the electrode–electrolyte interface. The shift of peaks toward higher frequencies was evident from plots. Values of dielectric constant on different temperatures and frequency are given in Table 4.

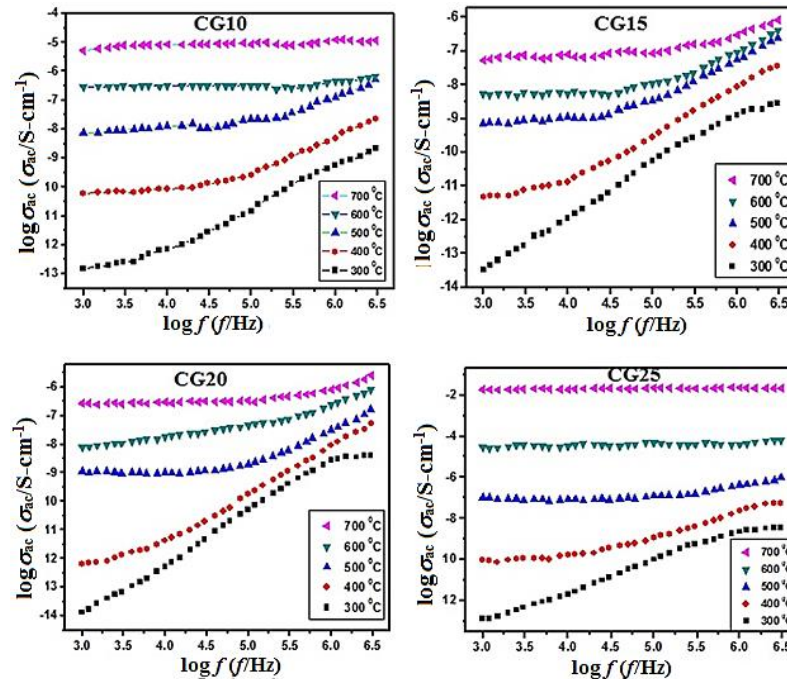


Fig. 5 AC conductivity as a function of frequency of $Ce_{1-x}Gd_xO_\delta$ ($x=0.10$ (CG10), 0.15 (CG15), 0.20 (CG20), 0.25 (CG25)) at different temperatures

Table 3. Values of AC conductivity at different temperatures on different frequency applied of $Ce_{1-x}Gd_xO_\delta$ ($x= 0.10$ (CG10), 0.15 (CG15), 0.20 (CG20), 0.25 (CG25))

Sample	AC conductivity ($S\cdot cm^{-1}$) at 3MHz			AC conductivity ($S\cdot cm^{-1}$) at 1kHz		
	500 °C	600 °C	700 °C	500 °C	600 °C	700 °C
CG10	0.0025	0.0023	0.0081	2.97×10^{-4}	0.0015	0.0051
CG15	0.0014	0.0017	0.0023	1.08×10^{-4}	2.59×10^{-4}	6.98×10^{-4}
CG20	0.0012	0.0023	0.0037	1.3×10^{-4}	3.04×10^{-4}	0.0014
CG25	0.0025	0.015	0.189	9.34×10^{-4}	0.0107	0.176

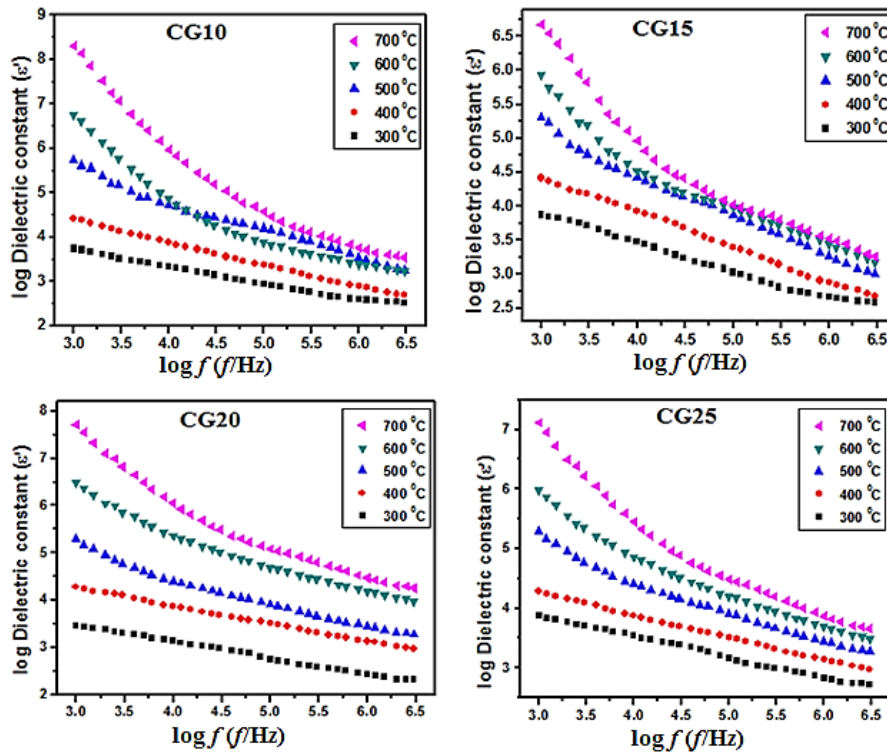


Fig. 6 Dielectric constant as a function of frequency of $Ce_{1-x}Gd_xO_\delta$ ($x= 0.10$ (CG10), 0.15 (CG15), 0.20 (CG20), 0.25 (CG25)) at different temperatures

Table 4: Values of Dielectric constant for different temperatures on different frequency applied of $Ce_{1-x}Gd_xO_\delta$ ($x= 0.10$ (CG10), 0.15 (CG15), 0.20 (CG20), 0.25 (CG25))

Sample	Dielectric Constant at 3MHz			Dielectric Constant at 1kHz		
	500 °C	600 °C	700 °C	500 °C	600 °C	700 °C
CG10	25.83	25.53	34.45	315.21	857.62	4077.75
CG15	20.22	24.05	26.06	202.21	375.91	794.14
CG20	26.62	32.45	38.85	200.46	398.12	1229.72
CG25	27.33	39.98	24.70	758.53	7033.89	108676.66

The frequency dependent $\tan\delta$ plots are given in Fig. 7 for $Ce_{1-x}Gd_xO_\delta$ ($x= 0.10, 0.15, 0.20, 0.25$). At lower frequencies, $\tan\delta$ has larger values and at higher frequencies, the values decreased and became independent of frequency due to the fact that the ions were not able to respond and reorient themselves with applied frequency. Also, the relaxation and reorientation peaks shifting

toward higher frequencies with increase in temperature is clear in plots. Values of $\tan\delta$ for different temperatures at applied frequency are shown in Table 5.

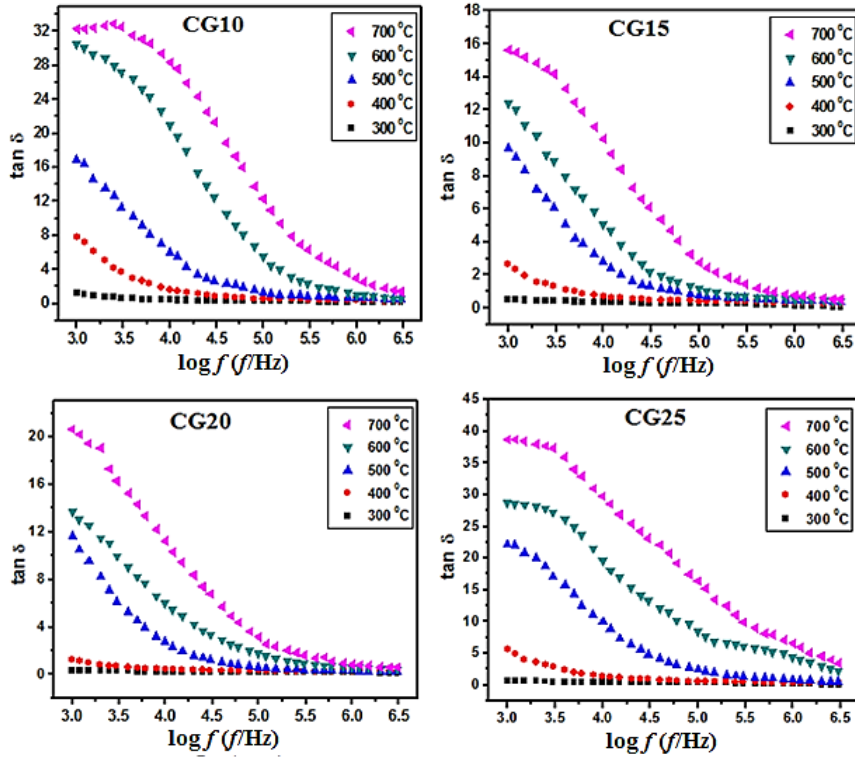


Fig. 7. Dielectric loss as a function of frequency of $Ce_{1-x}Gd_xO_\delta$ ($x = 0.10$ (CG10), 0.15 (CG15), 0.20 (CG20), 0.25 (CG25)) at different temperatures

Table 5. Values of $\tan\delta$ at different temperatures on different frequency applied of $Ce_{1-x}Gd_xO_\delta$ ($x = 0.10$ (CG10), 0.15 (CG15), 0.20 (CG20), 0.25 (CG25))

Sample	Dielectric loss ($\tan\delta$) at 3MHz			Dielectric loss ($\tan\delta$) at 1kHz		
	500 °C	600 °C	700 °C	500 °C	600 °C	700 °C
CG10	0.57	0.54	1.41	16.94	30.59	22.29
CG15	0.40	0.42	0.52	9.65	12.41	15.82
CG20	0.26	0.41	0.57	11.68	13.73	20.63
CG25	0.54	2.26	3.45	22.14	28.72	38.72

3.4. Thermal measurements

The room temperature thermal conductivity and thermal diffusivity values were measured using ATPS method. This method provides the simultaneous measurements of the conductivity and diffusivity. The values obtained are given in Table 6. The samples showed the values are in lower conductivity range. These low thermal conductivity samples can be utilized for the thermal barrier coatings. The conduction of heat inside solids is aided through the scattering of phonons. The decrease in conductivity with increase of Gd contents might be due to the increase of vacancies which slowed down the phonons. The increase of ionic conduction showed that the thermally activated ionic transport in these samples was not significant [40].

Table 6: Values of thermal conductivity and thermal diffusivity for $Ce_{1-x}Gd_xO_\delta$ ($x = 0.10$ (CG10), 0.15 (CG15), 0.20 (CG20), 0.25 (CG25)) at room temperature.

Sample	Thermal Conductivity $Wm^{-1}K^{-1}$	Thermal Diffusivity mm^2s^{-1}
CG10	0.42	0.64
CG15	0.15	0.91
CG20	0.39	0.71
CG25	0.40	0.79

4. Conclusions

Nanocrystalline gadolinium doped ceria, $Ce_{1-x}Gd_xO_\delta$ ($x = 0.10, 0.15, 0.20, 0.25$), were successfully synthesized with facile composite mediated hydrothermal method. The x-ray diffraction confirmed the phase and composition of the synthesized material. The crystallite sizes were estimated using Scherrer and Stokes and Wilson's formulae. The range of crystallite size was 30-83 nm corresponding to most intense peak using Scherrer's formula. The x-ray diffraction data was used to calculate lattice constants. The range obtained for lattice constant was 5.38 Å to 5.40 Å.

The scanning electron microscopy was used to get morphology of the materials. $Ce_{0.9}Gd_{0.1}O_\delta$ has needles like structures, whereas other three samples have coarse particles morphology. DC conductivity was measured in temperature range 300-700 °C. AC conductivity was calculated in frequency range 1 kHz to 3 MHz at temperatures 300, 400, 500, 600 and 700 °C. The larger values of conductivities were obtained for compositions $Ce_{0.9}Gd_{0.1}O_\delta$ and $Ce_{0.75}Gd_{0.25}O_\delta$. An increasing trend of conductivities was observed for increase in temperature. Arrhenius plots were used to calculate activation energies, obtained in the range 0.87-1.19 eV for 300-700 °C. The 'universal' dielectric response with Jonscher's law and jump relaxation model explained the conduction phenomena in the synthesized material.

The maximum conductivity was achieved for $Ce_{0.75}Gd_{0.25}O_\delta$ to be $9.30 \times 10^{-4} S\text{-cm}^{-1}$ at 600 °C. The thermal conductivity values for these samples lie in low thermal conductivity region and material could be utilized as thermal barrier coatings. The Raman spectroscopy seconded the structural, electrical and thermal results. The CMH method was found better synthesis method for electrolyte materials for ITSOFCs.

Acknowledgments

The assistance of CMND (for Raman measurements), Mr. M. Mubeen and Mr. S. Muzammil is appreciated. The Higher Education Commission Pakistan is acknowledged for financial support.

References

- [1] W. J. Bowman, J. Zhu, R. Sharma, P. A. Crozier, *Solid. State. Ionic.* **272**, 9 (2015)
- [2] A. B. Stambouli, E. Traversa, *Renew. Sust. Energ. Rev.* **6**, 433 (2002)
- [3] K. C. Wincewicz, J. S. Cooper, *J. Power. Sources.* **140**, 280 (2005)
- [4] J. Molenda, K. Swierczek, W. Zajac, *J. Power. Sources.* **173**, 657 (2007)
- [5] B. Zhu, *Int. J. Energy. Res.* **33**, 1126 (2009)
- [6] H. Jin, N. Wang, L. Xu, S. Hou, *Mater. Lett.* **64**, 1254 (2010)
- [7] S. Hui, J. Roller, S. Yick, X. Zhang, C. Deces-Petit, Y. Xie, R. Maric, D. Ghosh, *J. Power Sources.* **172**, 493 (2007)
- [8] E. Y. Pikalova, A. A. Murashkina, V. I. Maragou, A. K. Demin, V. N. Strekalovsky, P. E. Tsiakaras, *Int. J. Hydrogen. Energy.* **36**, 6175 (2011)

- [9] F. F. Munoz, A. G. Leyva, R. T. Baker, R. O. Fuentes, *Int. J. Hydrogen. Energy.* **38**, 14854 (2012)
- [10] J. Waldhäusl, W. Preis, W. Sitte, *Solid. State. Ionic.* **225**, 453 (2012)
- [11] L. Zhang, R. Lan, P. I. Cowin, S. Tao, *Solid. State. Ionic.* **203**, 47 (2011)
- [12] V. Shelukhin, I. Zon, E. Wachtel, Y. Feldman, I. Lubomirsky, *Solid. State. Ionic.* **211**, 12 (2012)
- [13] C. S. Riccardi, R. C. Lima, M. L. dos Santos, P. R. Bueno, J. A. Varela, E. Longo, *Solid. State. Ionic.* **180**, 288 (2009)
- [14] X. Li, Z. Feng, J. Lu, F. Wang, M. Xue, G. Shao, *Ceram. Int.* **38**, 3203 (2012)
- [15] Z. Khakpour, A. A. Youzbashi, A. Maghsoudipour, K. Ahmadi, *Powder. Technol.* **214**, 117 (2011)
- [16] E. Konysheva, T. S. J. Irvine, *Solid. State. Ionic.* **184**, 27 (2011)
- [17] S. A. Acharya, *J. Power. Sources.* **198**, 105 (2012)
- [18] Z. Shao, W. Zhou, Z. Zhu, *Prog. Mater. Sci.* **57**, 804 (2012)
- [19] E. Shoko, M. F. Smith, R. H. McKenzie, *J. Phys: Condens. Matter.* **22**, 223201 (2010)
- [20] D. A. Andersson, S. I. Simak, N. V. Skorodumova, I. A. Abrikosov, B. P. Johansson, *Natl. Acad. Sci.* **103**, 3518 (2006)
- [21] S. R. Bishop, K. L. Duncan, E. D. Wachsman, *Electrochim. Acta.* **54**, 1436 (2009)
- [22] P. P. Dholabhai, S. Anwar, J. B. Adams, P. A. Crozier, R. Sharma, *Modell. Simul. Mater. Sci. Eng.* **20**, 015004 (2012)
- [23] H. Liu, C. Hu, Z. L. Wang, *Nano. Lett.* **6**, 1535 (2006)
- [24] H. W. Otto, R. P. Seward, *J. Chem. Eng. Data.* **9**, 507 (1964)
- [25] http://www.crct.polymtl.ca/fact/phase_diagram.php?file=KOH-NaOH.jpg&dir=FTsalt
- [26] J. W. Mullin, *Crystallization*, 4th edn. Butterworth Heinmann, Oxford (2001)
- [27] M. Anis-ur-Rehman, A. Maqsood, *J Phys D: Appl. Phys.* **35**, 2040 (2002)
- [28] L. Li, F. Chen, J-Q Lu, M-F Luo, *J. Phys. Chem. A* **115**, 7972 (2011)
- [29] J. R. McBride, K. C. Hass, B. D. Pointdexter, W.H. Weber, *J. Appl. Phys.* **76**, 2435 (1994)
- [30] B. C. H. Steele, *Solid. State. Ionic.* **129**, 95 (2000)
- [31] R. K. Lenka, T. Mahata, A. K. Tyagi, P. K. Sinha, *Solid. State. Ionic.* **181**, 262 (2010)
- [32] A. S. Nowick, A. V. Vaysleyb, I. Kuskovsky, *Phys. Rev. B* **58**, 8398 (1998)
- [33] K. Funke, *Prog. Solid. State. Chem.* **22**, 111 (1993)
- [34] M. F. Gelin, D. S. Kosov, *J. Chem. Phys.* **130**, 134502 (2009)
- [35] A. K. Baral, V. Sankaranarayanan, *Appl. Phys. A* **98**, 367 (2010)
- [36] A. K. Jonscher, *J. Phys. D: Appl. Phys.* **32**, R57 (1999)
- [37] A. Baral, V. Sankaranarayanan, *Nanoscale. Res. Lett.* **5**, 637 (2010)
- [38] C. Veranitisagul, A. Kaewvilai, W. Wattanathana, N. Koonsaeng, E. Traversa, A. Laobuthee, *Ceram. Int.* **38**, 2403 (2012)
- [39] A. S. Saleemi, A. Abdullah, M. Anis-ur-Rehman, *J. Supercond. Nov. Magn.* **26**, 1065 (2013)
- [40] S. J. Litzelman, J. L. Hertz, W. Jung, H. L. Tuller, *Fuel. Cell.* **8**, 294 (2008)